Improvement of electromagnetic torque of BLDC motor for electrical cutter application

Muhammad Izanie Kahar[1,2], Raja Nor Firdaus Kashfi Raja Othman[1,2], Aziah Khamis[1,2],
Kasrul Abdul Karim[1,2], Fairul Azhar Abdul Shukor[1,2], Ahmad Fuad Ab Ghani[3], Rofizal Mat Rejab[4],

[1]Faculty of Electrical Technology and Engineering, Universiti Teknikal Malaysia Melaka (UTeM), Melaka, Malaysia
[2]Research Laboratory of Electrical Machine Design, Centre of Robotics and Automation (CeRIA), Universiti Teknikal Malaysia Melaka (UTeM), Melaka, Malaysia
[3]Faculty of Mechanical Technology and Engineering, Universiti Teknikal Malaysia Melaka (UTeM), Melaka, Malaysia
[4]RZTech Resources Sdn. Bhd., Kuala Lumpur, Malaysia

ABSTRACT

As the advancement of brushless direct current (BLDC) motor is rising, it has been an advantage to use the motor for a wide range of applications. Its robustness and torque development have benefited small applications, such as the agriculture cutter. However, dropping performances of conventional BLDC are affected by the shape of the rotor that has unused magnetic flux. Therefore, this research aimed to analyze the electromagnetic torque by reducing the unused flux from an electromagnetic point of view. Two BLDC models with different slot-pole numbers and rotor types were modeled and simulated with equal permanent magnet volume, and magnetomotive force (MMF). Finite element method (FEM) software was used to compute back-electromotive force (BEMF), cogging torque, electromagnetic torque, and magnetic flux density of the BLDC models. As a result, 9/8 slot-pole with zero ferromagnetic underneath the permanent magnet had the highest BEMF and torque produced compared to the conventional type, with a percentage difference of 27%. In conclusion, this research presents the motor that had an improvement of electromagnetic torque for electrical cutter application.

Corresponding Author:

Raja Nor Firdaus Kashfi Raja Othman
Faculty of Electrical Technology and Engineering, Universiti Teknikal Malaysia Melaka (UTeM)
76100, Durian Tunggal, Melaka, Malaysia
Email: norfirdaus@utem.edu.my

1. INTRODUCTION

Nowadays, the development of cutting machines has vastly grown to increase the chopping or cutting process, which could ease the user. With an advanced machine, the cutting rate process or production could be increased while reducing the labour work, which could save time and costs. Different motors like induction motor (IM), linear motor, permanent magnet synchronous motor (PMSM), and direct current motor (DC) can be used in cutting machinery [1]–[5]. However, brushless direct current (BLDC) motor shows better efficient performance and abilities. It has high robustness, sturdy and simple structure that enables highly efficient operation, high torque, and less noisy operation [6]–[8]. Therefore, BLDC is a suitable motor for electrical cutter applications.

However, some BLDC applications had a downturn as several factors led to some cutting issues in the motors. When it comes to the BLDC motor, high torque is necessary for the cutting process [9]–[11]. Due to the limitation of height use and hardness of an object, the motor loses its cutting capabilities. As this could also be affected by the structure and construction of the stator and rotor itself, an improper structure might

cause the motor to lose its magnetic energy [12]–[14]. Therefore, resulting in a smaller value of torque. Although almost all BLDC motors have similar construction of stators, the rotor construction itself makes each of them unique. The direction of magnets, air-gap length, and type of rotor are the key factors that contribute to the efficiency of BLDC motors [15], [16]. Moreover, these rotor constructions could be the way to counter the problems that are being faced, which is way better than using an expensive rare-earth permanent magnet.

Therefore, these issues lead to some researchers to modify and improve the rotor to achieve better torque. For instance, research was done by [17]–[19] on irreversible demagnetization in the rotor structure. According to the authors, the reluctance torque had a significant impact on torque characteristics. Taking this factor into account, the magnetic flux density proportionally increased the torque. Meanwhile, Kim *et al.* [18] analyzed the dynamic characteristics of irreversible demagnetization in surface-mount permanent magnet (SPM) and interior permanent magnet (IPM) rotor types. They stated that the structure of the rotor influenced the direction or the line spread of magnetic flux. This means that the wide space of the rotor caused a reduction in back-electromotive force (BEMF) and output torque. Therefore, the motor performances were extremely degraded [20]. Another researcher, Zheng *et al.* [20] proposed new IPM rotor topologies to overcome the low torque reluctance and flux weakening problems. By doubling the permanent magnets and arranging them in U- and V-shape, the maximization of reluctance torque was achieved. However, there is unneeded space in the rotor that causes the wasted flux to be spotted [21]. Meanwhile, Lee *et al.* [21] conducted a comparative study on the BLDC motor under various operating conditions. The author employed a strategy for improving torque characteristics by designing flux barriers. With this alternative, the air gap caused the magnetic flux to be concentrated and the torque was maximized by the flux barrier [22], [23]. On the other hand, Kim *et al.* [23] proposed a new spoke-type BLDC rotor shape without replacing or modifying the ferrite magnet. To counteract the poorer torque of conventional ferrite magnet motors, the author minimized the bridge between the shaft and rotor core located under the magnet. By using this method, the thin bridge minimized the magnetic flux leakage, thus increasing the torque value [24].

The authors concluded a hypothesis that excessive space of the rotor could affect the magnetic flux, thus worsening the torque performance of the motor. For such reason, it is considered to completely minimize the space of the rotor under the permanent magnets which could optimize the magnetic flux and eliminate any flux leakage. Therefore, this research concentrated on improving the electromagnetic torque of BLDC by optimizing the magnetic flux in the rotor. Two types of rotors, which are conventional and hollow, that have zero ferromagnetic material underneath the permanent magnet with equal sizing and magnet volume were used for the research. Finite element method (FEM) was used to compute the magnetic characteristic simulation and analysis for the torque development of the BLDC for the electrical cutter application.

2. STRUCTURE OF PM BLDC

In this research, the example of the cutter given was for oil palm cutter application, as shown in Figure 1. By considering the maturity of the oil palm frond, a 1 nm motor is enough for the cutting process [25]. Target specifications of the BLDC motor are shown in Table 1. It is a 3-phases motor that is supplied by 36 vdc. Its rotational speed is expected to be 1,800 rpm, whereby its BEMF should be as bigger as possible but below the supply voltage. Furthermore, to obtain cutting torque as required, the rotational speed should be low, but adequate to main the rate of the cutting process. A model was chosen by its performance based on the required specifications.

Figure 1. Example application for this motor [26]

Table 1. PM BLDC design specifications

Target design specifications		Value
Input voltage, V	[V]	36
No. of phases		3
Rotational speed, ω	[rpm]	1,800
Torque required, τ	[Nm]	> 1.0

The slot-pole configuration used was 9/8 slot-pole based on fractional slots, and 3-phase windings topology. Since the aim was to have higher cutting torque, 6/4 slot-pole was not suitable. Increasing pole number to more than 8 was impractical since the rotor diameter was small. Figure 2 shows the block diagram for the electrical cutter application implemented in this research. The DC input power supply was converted into AC by the electronic circuit and driver which allowed the motor to operate in a 3-phase system. With the aid of the Hall sensor, the initial position of the rotor was determined to obtain the highest torque produced. The driver control received signals from the Hall sensor and the position of the rotor was adjusted to match the Hall signal with the BEMF. Sinusoidal BEMF was expected to be the feature in this research.
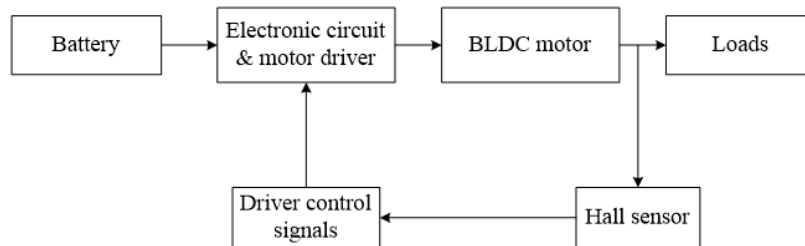
Figure 2. Example of block diagram system

2.1. Basic structure of conventional and proposed hollow rotor

Initially, the structures of both rotors were almost the same. Except that, the excessive ferromagnetic material underneath the permanent magnet was reduced, as shown in Figure 3. In conventional rotor, the flux flowed around the permanent magnet and stator yoke, indicating unused flux passing through the end of the permanent magnet as excessive ferromagnetic material formed on the rotor as shown in Figure 3(a). This demonstrated that the unused flux was squandered and not adequately optimized; hence it did not contribute to torque production.

In contrast to the hollow rotor, its inner radius was created to be as large as the end of the permanent magnet, as seen in Figure 3(b). This implied that there was no extra ferromagnetic material as in a conventional rotor. As a result, there was no flux leakage, and the magnetic flux of the permanent magnet had been thoroughly optimized, potentially increasing torque production. The rotor's shape is crucial and can significantly impact the motor's performance. Without the occurrence of wasted flux, the hollow rotor was expected to produce more torque than the conventional rotor.
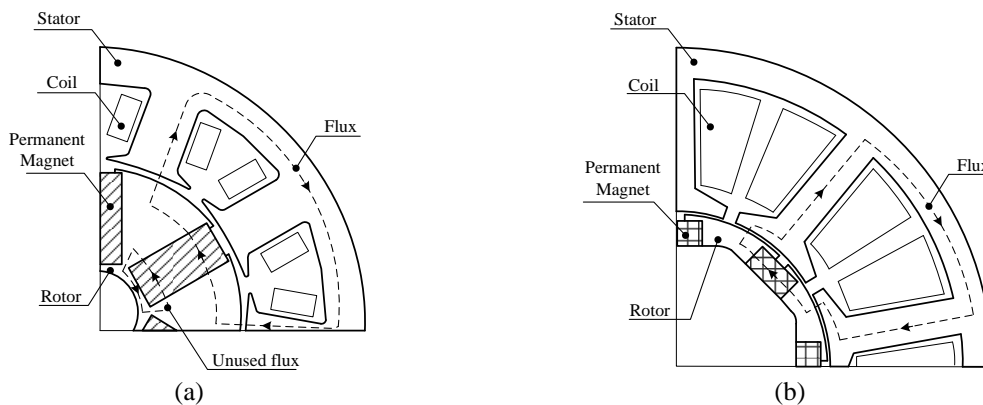
Figure 3. Basic structure of (a) conventional [27] and (b) hollow rotor [28]

2.2. Motor sizing

In this paper, the number of turns was varied with three different values, and the rotors used two different sizes of the permanent magnet to develop the model's sizing. The dimensions and parameters are shown in Figure 4. The 9/8 slot-pole model is developed, as shown in Figure 4. Except for the rotor inner radius, which had differences throughout the procedure, the models were developed with fixed parameters, such as stator and rotor outer radius, air gap, stack length, and permanent magnet volume.
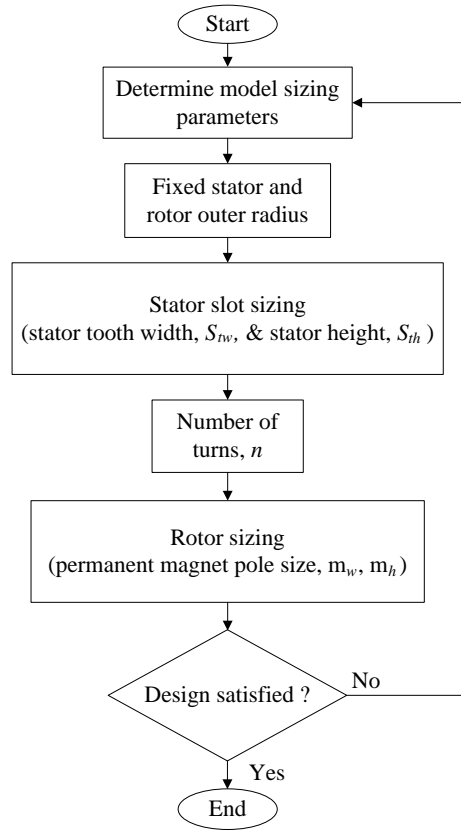
Figure 4. Flowchart of motor sizing in this research

2.2.1. Stator design

Figure 5 shows the stator sizing of the motor in this research. The stator dimension was determined using the conventional design method [28]. Starting with the stator, its outer sizing was fixed for all models with an inner radius set to 18 mm. Then, the dimensioning proceeded with the stator tooth height, S_{th}, which was calculated as in (1). The stator tooth height was considered to be half of the stator tooth width, S_{tw}. The flux, $\Phi 1$, from the permanent magnets, split and flowed through the stator yoke, shown as flux $\Phi 2$. Therefore, the stator tooth height depended on the value of stator tooth width, as shown in Figure 5(a).

Next, the number of turns winding, which depends on the coil size, cs, was defined using (2) and (3). Where nh and nw were the turns that fit along with the height and width of the stator slot, respectively. The coil fill factor was fixed at 60%. While Figure 5(b), shows the slot height, sh and slot width, sw. During the winding turns calculation, these models were varied with three different values of turns, whereby all had equal magnetic energy.

$$S_{th} = \frac{1}{2} \times S_{tw} \text{ [mm]} \tag{1}$$

$$\text{Turn}, n = (n_h)(n_w) \times 60\% \text{ [turns]} \tag{2}$$

$$n_h = \frac{s_h}{c_s} , \ n_w = \frac{s_w}{c_s} \text{ [mm]} \tag{3}$$
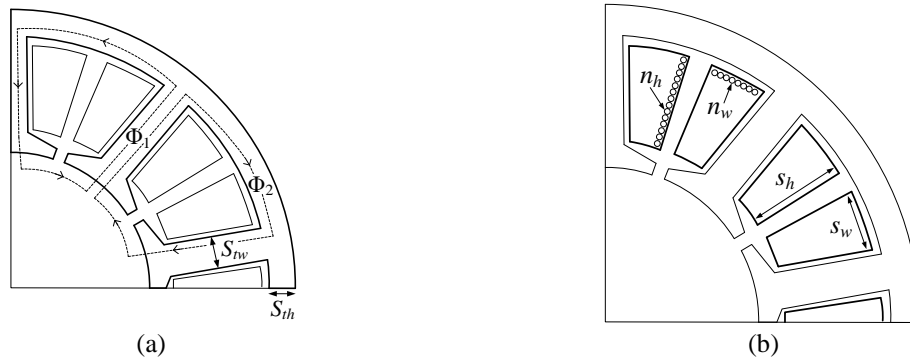
Figure 5. Stator sizing (a) stator tooth width, S_{tw} & stator tooth height, S_{th} and (b) slot height, s_h & slot width, s_w

2.2.2. Rotor design

The design of the rotor included the dimension of outer diameter, air gap length, and permanent magnet sizing. For all models, the outer diameter was fixed at 17.5 mm with an air gap between the rotor and stator fixed to 0.5 mm. For permanent magnet sizing, the shape used for both conventional and hollow rotors was rectangular, and the dimensions are shown in Figure 6, where mh is permanent magnet height while mw is permanent magnet width. The sizes were chosen to be maximally fit in the rotor and by considering excess space between the end of the permanent magnet and the shaft radius. Both models had two different sizes of permanent magnets but with an equal volume between the two models. Neodymium boron iron (NdFeB) was the material chosen for the permanent magnets of the rotor core.

Figure 7 shows rotor sizing of the motor in this research. The components that differentiated between the conventional and hollow rotor was the ferromagnetic material below the permanent magnets. Figure 7(a) shows the conventional rotor with its inner radius of 7 mm, allowing the magnetic flux to circulate through the end of the permanent magnets, and Figure 7(b) shows the hollow rotor without the excessive ferromagnetic material.
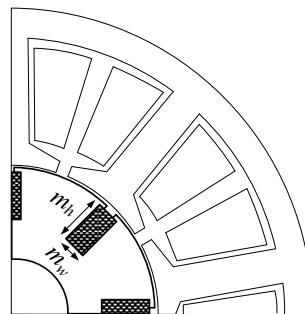
Figure 6. Permanent magnet sizing

Figure 7. Rotor sizing (a) conventional rotor and (b) hollow rotor

Table 2 shows the tabulated parameters of the designed BLDC models. The stator and rotor sizing, stack length, and air gap value were kept the same. The air gap prevented the stator and rotor from colliding with each other. Furthermore, the air gap value was set to be 0.5 mm to ensure an efficient flow of magnetic flux between the permanent magnets and stator. The permanent magnet volume and magnetic energy of the windings were kept the same for both models to analyze the effects and performances based on the same torque volume.

Table 2. Designed parameter of PM BLDC motor for two different slots and poles

Parameter		Motor 1	Motor 2
Slots and poles number		9/8	
Stator slot		9	
Winding turns	[turns]	15	
		30	
		60	
Input current	[A]	2.5, 5, 7.5, 10, 12.5	
Air gap	[mm]	0.5	
Rotor type		Conventional	Hollow
Pole number		8	
Rotor inner radius	[mm]	0.8 mm below permanent magnet	End-of-permanent magnet
Magnet type		Not embedded	
Permanent magnet volume	[mm^3]	15008 (PM 1)	
		10528 (PM 2)	

3. ELECTROMAGNETIC ANALYSIS OF CONVENTIONAL AND PROPOSED HOLLOW ROTOR

Figure 8 shows the structure of 9/8 slot-pole configuration and magnetic flux of conventional and hollow rotors simulated using FEM. With FEM, the system could give expected visual output efficiently with high accuracy. Both models were varied with three different values of turns, which were 135, 270, and 540 turns, and two sizes of permanent magnets with 2 mm differences were used. The permanent magnet material was neodymium iron boron (NdFeB), and the stator and rotor were made up of silicon steel. Figure 8(a) shows the BLDC with the conventional rotor with a round edge at the inner diameter. Compared with the hollow rotor with flat edges, the models eliminated the excessive ferromagnetic material, which made its inner diameter less 0.8 mm, as shown in Figure 8(b).

The rotor was made up of silicon steel, allowing the magnetic flux to flow. As the conventional rotor has an excess area below the end of the permanent magnets, it allows some flux to circulate in the area without reaching the stator, as shown in Figure 8(c). This factor is the reason for flux leakage or unused flux to occur. Therefore, the BLDC motor performance was not optimally achieved as the unused flux was wasted and did not contribute to the torque generation. Therefore, to overcome the situation, the area below the permanent magnets was kept completely hollow. As a result, the excess area was eliminated, hence no flux leakage occurred, as shown in Figure 8(d). From the figures, it can be seen the flux lines was being optimally used when it flowed to other areas of the rotor. With all the magnetic fluxes being fully optimized and flowing through the stator, the torque value could increase and contribute to the performance of the BLDC motor.

In this research, BEMF and cogging torque were varied ranging from 600 rpm, 1,200 rpm, 1,800 rpm, and 2,400 rpm with zero input current. Then, these models proceeded to constant speed and static torque computation to analyze the electromagnetic torque and magnetic flux density at the stator. During this computation, the input current ranged from 2.5 A, 5 A, 7.5 A, 10 A, and 12.5 A with a constant speed of 1,800 rpm, as stated in the design specifications. Finally, the results were grouped by permanent magnet volumes, which were 15,008 mm^3 for PM 1 and 10,528 for PM 2. At the end of the analysis, the performance of each model was evaluated to be suited for the desired specifications of the electrical cutter applications.

3.1. Result of back electromotive force, back-EMF

Figure 9 shows the RMS values of BEMF for both hollow and conventional rotor types under speeds ranging from 600 rpm, 1,200 rpm, 1,800 rpm, and 2,400 rpm. During this computation, current excitation was not required, thus input current was set to 0 A. In this state, the motor was corresponded to be in generator mode with a no-load connection. As illustrated, the BEMF for all these models increased linearly with the rotational speed. The models with conventional rotors were maintained to be the lowest. The permanent magnet volume and number of turns could give a major influence on the BEMF produced.

Figure 9 illustrates the BEMF value against rotational speed with different number of turns which were 15, 30, and 60 turns. Figure 9(a) shows the BEMF value for BLDC models with PM 1. At the lowest

speed of 600 rpm, the BEMF values achieved by the conventional rotor model for 15, 30, and 60 turns were 4 V, 8 V, and 16 V, respectively. Meanwhile, the hollow rotor model achieved 5 V, 10 V, and 20 V higher than the conventional rotor. The BEMF increased steadily with the rotational speed until 2,400 rpm. At 2,400 rpm, the BEMF values for the conventional model with 15, 30, and 60 turns were 16 V, 32 V, and 63 V, respectively. Meanwhile, the hollow model achieved 20 V, 40 V, and 80 V higher than the conventional rotor. The percentage difference between conventional and hollow models was maintained to be 27% along with the increment. Next, Figure 9(b) shows the BEMF for models with PM 2. At 600 rpm, for 15, 30, and 60 turns, the conventional model obtained 3 V, 5 V, and 10 V, respectively. Meanwhile, the hollow model achieved 4 V, 8 V, and 15 V higher than the conventional rotor. The value steadily rose until the rotational speed of 2,400 rpm. At 2,400 rpm, the BEMF values for the conventional model with 15, 30, and 60 turns were 10 V, 21 V, and 42 V, respectively, while, the hollow model achieved 15 V, 31 V, and 61 V higher than the conventional rotor. The percentage difference of both conventional and hollow rotor was maintained to be 47%.
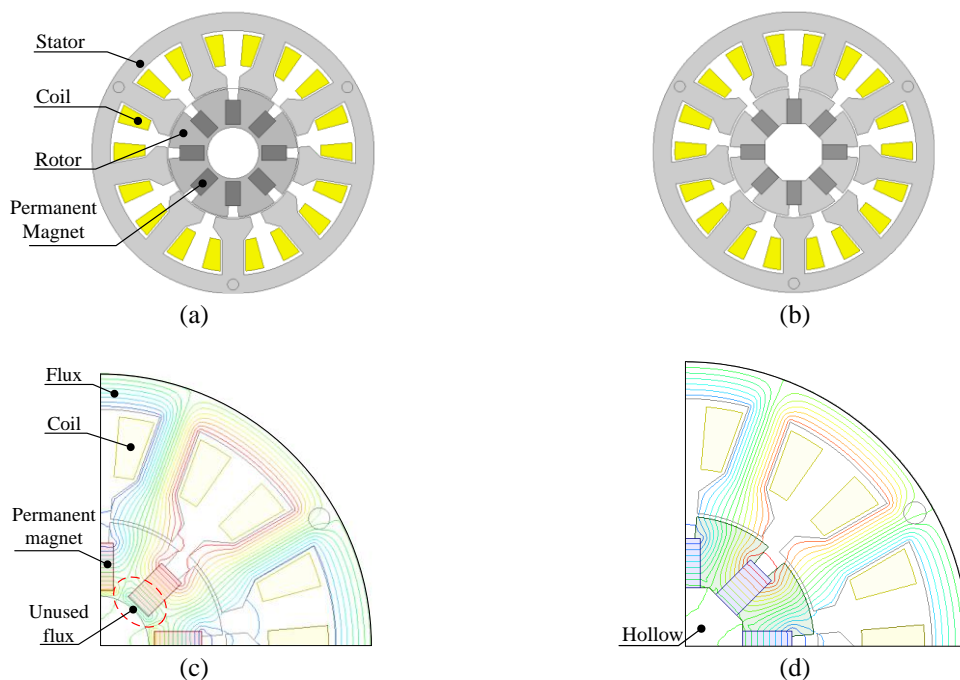
Figure 8. Designed PM BLDC structure with two different rotors: (a) 9/8 slot-pole with conventional rotor (motor 1), (b) 9/8 slot-pole with hollow rotor (motor 2), (c) conventional rotor (motor 1), and (d) hollow rotor (motor 2)

It can be seen that the size of the permanent magnet had a major effect on the BEMF produced. Bigger permanent magnet volume contributed to higher BEMF produced due to higher magnetic energy causing strong attraction between the stator and rotor, thus causing the stator and rotor to be rotated easily. With slight differences of 2 mm, the percentage differences of BEMF for the conventional and hollow rotor model between PM 1 and PM 2 were 27% and 47%, respectively. BEMF values were also affected by the number of turns. Higher number of turns produced higher magnetic energy and flux, which attracted the magnetic flux from the rotor and caused it to rotate efficiently. Therefore, the higher number of turns used, the higher BEMF will be produced. The BEMF increased linearly with the rotational speed due to the rate of change of magnetic flux between the stator and rotor. This means that the rate at which the magnetic flux from the stator attracted the magnetic flux from moving permanent magnet influenced the generated BEMF. Therefore, the greater the speed, the greater the magnitude of the BEMF will be. Furthermore, the shape of the rotor played an important role in generating BEMF. The magnetic flux was fully optimized with a hollow rotor and flowed all around the stator. Therefore, the induced voltage generated was higher than the conventional rotor model. As expected, the hollow rotor model with PM 1 had the highest BEMF due to the fully optimized magnetic flux in the hollow rotor and the bigger size of the permanent magnet used, thus, allowing it to produce the highest induced voltage compared to the other models.
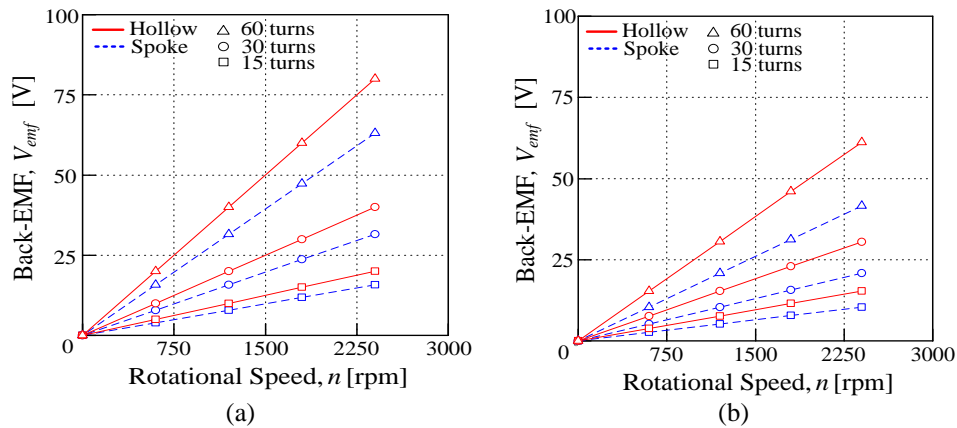
Figure 9. Back electromotive force, back-EMF (a) PM 1 and (b) PM 2

3.2. Result of cogging torque, T_C

This computation condition of cogging torque was similar to BEMF in which the excitation current was not required. The speed had a range of 600 rpm, 1200 rpm, 1,800 rpm, and 2,400 rpm. The cogging torque was simulated with varied positions for zero input current. However, the varied speed did not affect the cogging torque. Therefore, the result was selected at a speed of 1,800 rpm only.

Figure 10 illustrates the waveforms and values of cogging torque during speed of 1,800 rpm. Figure 10(a) shows that the waveforms and values for both conventional and hollow models were the same. Although the waveforms were not in the same magnitude, the RMS values of both cogging torque were equal. Figure 10(b) shows the cogging torque of hollow rotor model, which was higher than the conventional rotor. As shown, the amplitude of cogging torque in the hollow rotor was higher than in the conventional rotor, which means that there were higher differences in both values. From the result obtained, both models with PM 1 had the highest cogging torque of 0.02 nm, whereas cogging torques of the model with the conventional and hollow rotor of PM 2 were 0.006 nm and 0.017 nm, respectively. This trend continued as the rotational speed increased.

The dimensions of permanent magnet with rotor and stator structure could have caused uneven peak occurrence. In the aspect of slot opening width or the air gap length, the non-uniform air gap between the rotor and stator could have occurred. The disrupted air gap caused the rotor and stator to collide with each other; thus, causing the motor to experience more cogging torque and affecting its performance. Moreover, the rotational speed increment did not affect the cogging torque increment. It is due to the magnetic energy and attraction that was influenced by the magnetic flux density that flowed all around the rotor and stator. Therefore, as the hollow rotor optimized the magnetic flux and has stronger attraction, its cogging torque was higher than the conventional rotor model. Therefore, bigger size of the permanent magnet and structure of the rotor could influence the cogging torque to become higher.
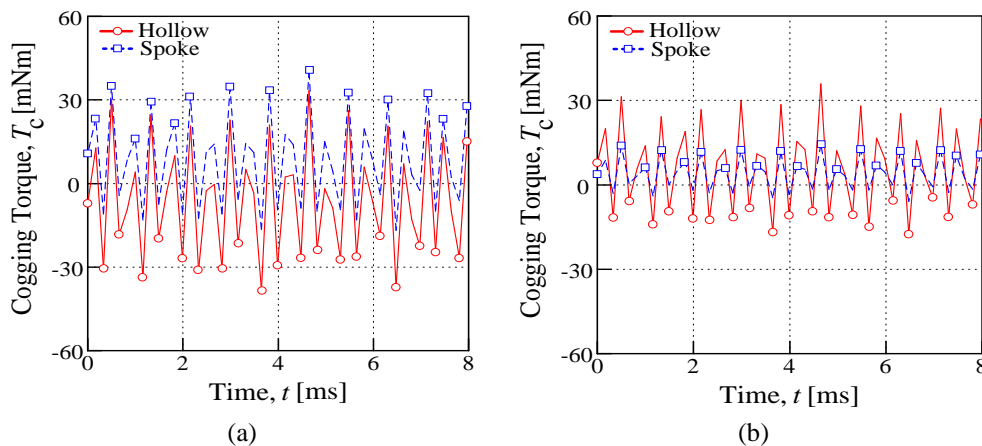
Figure 10. Cogging torque, T_C (a) PM 1 and (b) PM 2

3.3. Result of electromagnetic torque, T_e

For electromagnetic torque, the current source was required and simulated by using constant speed computation. This simulation was fixed at a constant speed of 1,800 rpm with various input currents. Then, the current firing angle obtained in the BEMF analysis was used in this simulation to achieve the maximum torque that it can produce. Therefore, the phase input current could be ensured to be aligned with the BEMF to obtain a high torque value. The input current values used for this computation were 2.5 A, 5 A, 7.5 A, 10 A, and 12.5 A. The final torque comparison among the models was made during the input current of 10 A, as required in the design specifications.

Figure 11 illustrates the average electromagnetic torque value produced by all models against the input currents (ranging from 2.5 A to 12.5 A). Figure 11(a) presents the electromagnetic torque values for conventional and hollow rotor models with PM 1. During input current of 2.5 A, for 15, 30, and 60 turns, the values for conventional rotor model were 0.27 nm, 0.54 nm, and 1.07 nm, respectively, meanwhile, for the hollow model, the values were 0.34 nm, 0.68 nm, and 1.35 nm, respectively, which were higher than the conventional model. These values increased until the highest input current of 12.5 A. At 12.5 A, the conventional model continued to be 1.33 nm, 2.54 nm, and 4.10 nm, respectively. Meanwhile, the hollow model achieved 1.67 nm, 3.16 nm, and 5.25 nm higher than the conventional model. The percentage difference between conventional and hollow at 2.5 A was 26% and increased slightly at 12.5 A, which was 28%. Figure 11(b) shows the value for models with PM 2. During input current of 2.5 A, for 15, 30, and 60 turns, the conventional model obtained 0.18 nm, 0.36 nm, and 0.72 nm, while the hollow model achieved 0.26 nm, 0.53 nm, and 1.05 nm, respectively. The value continued to rise until the input current of 12.5 A. At 12.5 A, the values for the conventional model with 15, 30, and 60 turns were 0.90 Nm, 1.78 Nm, and 2.80 Nm, respectively, while the hollow model achieved 1.31 nm, 2.51 nm, and 4.12 nm, respectively. The percentage difference of both conventional and hollow rotor models during input current of 2.5 A was 45.8%, and slightly increased at 12.5 A, which was 47.1%.

As illustrated in the figures, the electromagnetic torque produced by all models was nearly the same during low input current and it increased rapidly when the input current was higher. At this moment, when the input current increased, the coil winding was energized and produced electromagnetic energy. When a higher current was supplied, higher magnetic energy was produced. As a result, the electromagnetic produced interacted with the flux of permanent magnets. Therefore, as the hollow rotor fully optimized the magnetic flux, it had higher torque than the conventional rotor model. It can be seen that the electromagnetic torque obtained for all models increased linearly proportional to the input current. At the input current of 5 A, the torques of both conventional and hollow rotor models started to have a bigger difference between each other. At 10 A, the torque for the hollow rotor model with PM 1 was the highest, while the conventional rotor model with PM 2 had the lowest. As expected, the BEMF gave major influences on the motor. The model with the higher BEMF had higher electromagnetic torque value. The shape of the rotor also played an important role to fully optimize the magnetic flux in the motor; thus, contributing to higher torque generation.
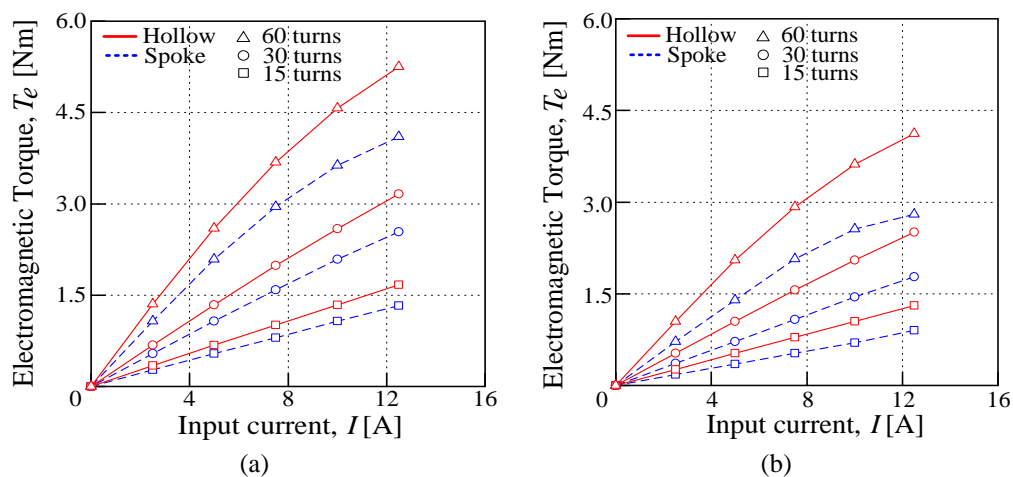
Figure 11. Electromagnetic Torque, T_e (a) PM 1 and (b) PM 2

3.4. Result of magnetic flux density, B

In this simulation, the magnetic flux density was analyzed by executing the values with the plot of colour shadings. Once the simulation was completed, all parts of the model were observed for its magnetic flux density. The analysis was done by matching the selected part of the model's face region with the colour shading plot to be analyzed. In this research, the middle of the stator tooth used for coil windings with the highest value was the region selected for the analysis. The magnetic flux density was significantly influenced by the changes in input current. Therefore, the input current values used for this analysis were 2.5 A, 5 A, 7.5 A, 10 A, and 12.5 A. The magnetic flux density values started to saturate at 1.9 T for all models.

Figure 12 shows the magnetic flux density obtained for all models against the input currents. It shows that the magnetic flux density for all models increased as the current input increased with similar patterns. As shown in Figure 12(a), during input current of 2.5 A for 15, 30, and 60 turns, the values for the conventional rotor model were 1.32 T, 1.43 T, and 1.59 T, respectively. Meanwhile, the hollow rotor produced 1.59 T, 1.65 T, and 1.75 T higher than the conventional model. The value increased until the highest input current of 12.5 A. At 12.5 A, the conventional rotor model achieved 1.66 T, 1.86 T, and 2.06 T, respectively, meanwhile, the hollow rotor produced 1.79 T, 1.93 T, and 2.1 T higher than the conventional model. Figure 12(b) shows that during input current values of 2.5 A for 15, 30, and 60 turns, the values for the conventional rotor model were 0.91 T, 1.04 T, and 1.27 T, while the hollow rotor produced 1.29 T, 1.39 T, and 1.56 T, respectively. The value continued to increase until input current of 12.5 A. At input current of 12.5 A, the conventional rotor model achieved 1.37 T, 1.75 T, and 2.03 T, while the hollow rotor produced 1.62 T, 1.84 T, and 2.06 T, respectively.

As tabulated in the figures, the hollow rotor model with PM 1 had the highest magnetic flux density, while the conventional rotor model with PM 2 had the lowest. For models with PM 1, the value increased minimally from the start until the end and saturated at 1.9 T. For models with PM 2, the hollow model increased gradually compared to the conventional rotor model. This shows that the hollow rotor model started at a higher value, increased slowly, and closed to the saturation point due to the fully optimised magnetic flux in the rotor.

It was concluded that the magnetic flux density could be affected by the number of coils turns. The greater number of the turns, the higher value of magnetic energy will be produced. The magnetic flux density could be increased together with the required input current. Therefore, higher magnetic flux density could contribute to higher torque generation.
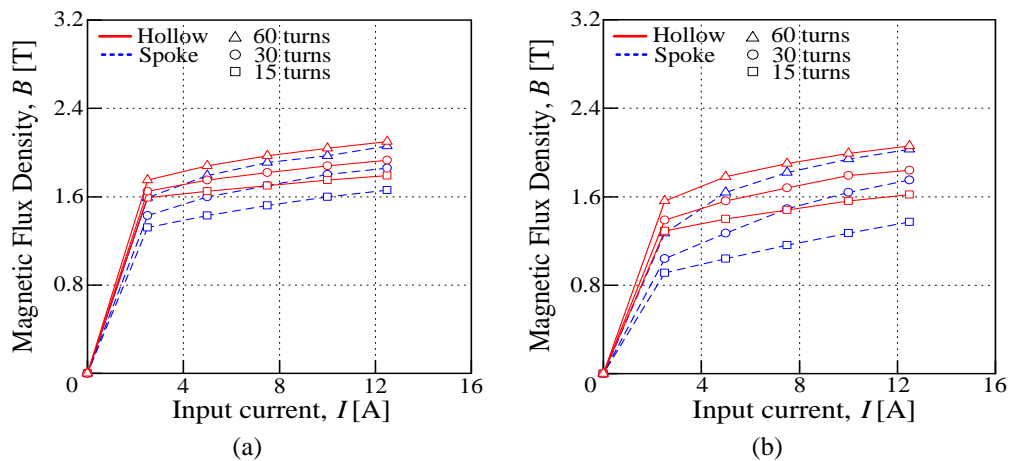
Figure 12. Magnetic flux density, B (a) PM 1 and (b) PM 2

3.5. Performance comparison

Table 3 shows the summary and comparison results for all models during certain conditions. The results presented are for 30 turns. The BEMF and cogging torque results were chosen at a rotational speed of 1,800 rpm, while the electromagnetic torque and magnetic flux density were based on the input current of 10 A. It was found that the proposed hollow rotor model with PM 1 was the best model for selection. By focusing on the values of BEMF, it had the highest value, which was able to contribute to the electromagnetic torque generation, thus obtaining the highest value torque among other models. Moreover, its cogging torque was maintained to be the same as the conventional rotor with PM 1 model; however, this issue did not seem to cause any major problem that could deteriorate the performance. Its magnetic flux was also the highest,

which showed that the magnetic flux in the rotor was fully optimized, and optimum magnetic energy was achieved. The second highest performance was of the conventional rotor with PM 1 model. The percentage difference of both conventional and hollow rotor for BEMF was 26.7%, while for electromagnetic torque, it was 23.9%. Therefore, with the high difference gap between them, the proposed hollow rotor model with PM 1 was selected as the most suitable model for the electric cutter motor application.

Table 3. Comparison on model selection

Parameters		Conventional (motor 1)		Hollow (motor 2)	
		PM 1	PM 2	PM 1	PM 2
Back-EMF, V_{emf}	[V]	24	16	30	23
Cogging torque, T_c	[Nm]	0.02	0.006	0.02	0.017
Electromagnetic torque, T_e	[Nm]	2.10	1.50	2.60	2.10
Magnetic flux density, B	[T]	1.80	1.64	1.88	1.79

3.6. Torque-speed characterization

Figure 13 shows the average torque against speed characterization of the selected model, whereby the hollow rotor was compared with the conventional rotor with both using PM 1 model. Based on Figures 13(a) and 13(b), when 36 V was applied, the stall torque values, Tstall produced with 15, 30, and 60 turns for the conventional rotor model were 1.7 nm, 5.9 nm, and -9.8 nm, while for hollow rotor were 2.3 nm, 15 nm, and -5.9 nm when the motor is at a standstill. This was the point at which the torque and current were maximized. On the other side, the values of no-load speed, ωno-load for 15, 30, and 60 turns for the conventional rotor model were 5,143 rpm, 2,769.2 rpm, and 1,384.6 rpm, while for hollow rotor were 4,500 rpm, 2,117.6 rpm, and 1,091 rpm. This was the maximum speed that the motor could achieve at a given voltage, which occurred in idealized cases where no torque was generated.

As can be seen, torque values of 60 turns were below 0 nm. This was because the BEMF generated was more than the supplying terminal voltage. At this condition, this machine acted as a generator. While for 15 turns, the no-load speed was much too far from the targeted rotational speed of 1,800 rpm and its stall torque was too low; thus the torque produced made the model unsuitable for cutting applications. Therefore, the model with 30 turns was selected.

(a) Motor 1   (b) Motor 2
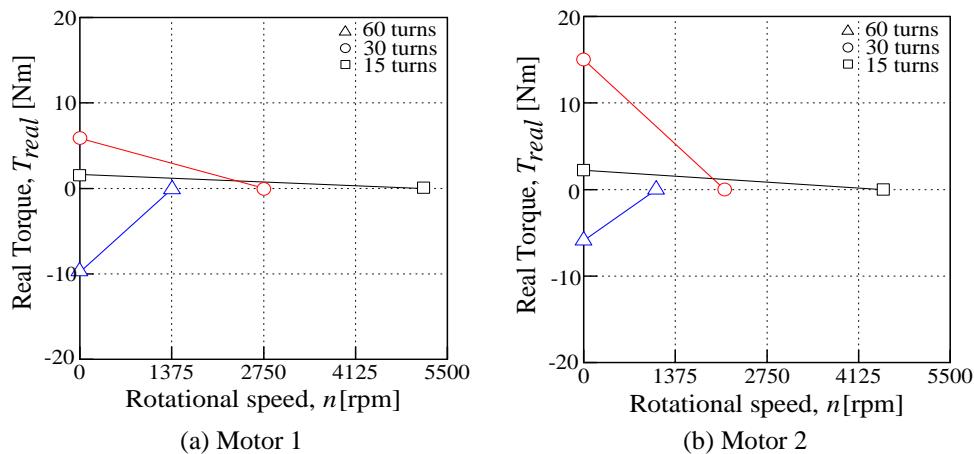
Figure 13. Torque-speed characterization of PM 1 models, (a) conventional (motor 1) and (b) hollow (motor 2)

4. CONCLUSION

The proposed models, which were the conventional and hollow rotor, were designed and simulated with fixed outer sizing, air gap, and slot-pole number. The analysis of transient magnetic application was carried out using FEM. The evaluation to select the best model focused on the highest BEMF and electromagnetic torque values. The BLDC motor with hollow rotor was found to be the best model. Based on the hollow rotor model characteristics with PM 1 and 30 turns, the BEMF generated was not more than 36 Vdc, as targeted. The torque achieved was more than 1 Nm, as required in design specifications. Meanwhile, with only 0.8 mm differences in the rotor inner radius, high gap differences were produced

between the conventional and hollow rotor performances. Therefore, this research showed that the performances of the BLDC motor were influenced by the shape of the rotor. The magnetic flux was fully utilized by optimizing the rotor shape, and the magnetic energy was optimally achieved. Therefore, the torque of the BLDC motor was improved. Based on the findings of this research, with the ability and good performances of this hollow rotor, future research could be conducted on the suitability for wood or steel cutting. To sum up, with efficient performances of the hollow rotor, it is possible for the BLDC motor to be used in the electric cutter application.

ACKNOWLEDGEMENTS

REFERENCES

[1] T. Khaorapapong and P. Ariyadirck, "Application of fuzzy logic in the position control of induction motor for bending and cutting machine," in *IEEE International Symposium on Communications and Information Technology, 2004. ISCIT 2004.*, 2004, vol. 1, pp. 378–382, doi: 10.1109/ISCIT.2004.1412872.

[2] K. Baluprithviraj, R. Harini, M. Janarthanan, and C. Jasodhasree, "Design and development of smart lawn mower," in *2021 2nd International Conference on Smart Electronics and Communication (ICOSEC)*, Oct. 2021, pp. 1215–1219, doi: 10.1109/ICOSEC51865.2021.9591825.

[3] M. A. Basunia and N. A. F. Narawi, "Improvement of grass cutting machine commonly used in Brunei," in *7th Brunei International Conference on Engineering and Technology 2018 (BICET 2018)*, 2018, pp. 1–4, doi: 10.1049/cp.2018.1565.

[4] N. Misron, U. Zanil, and S. S. Mustafa, "Linear oscillatory actuator integrated with magnetic gear for E-cutter development," in *2017 11th International Symposium on Linear Drives for Industry Applications (LDIA)*, Sep. 2017, pp. 1–5, doi: 10.23919/LDIA.2017.8097261.

[5] I. Zamudio-Ramirez, R. A. Osornio-Rios, G. Diaz-Saldana, M. Trejo-Hernandez, and J. A. Antonino-Daviu, "STFT-based induction motor stray flux analysis for the monitoring of cutting tool wearing in CNC machines," in *IECON 2020 The 46th Annual Conference of the IEEE Industrial Electronics Society*, Oct. 2020, pp. 2511–2516, doi: 10.1109/IECON43393.2020.9254795.

[6] S. J. Park, H. W. Park, M. H. Lee, and F. Harashima, "A new approach for minimum-torque-ripple maximum-efficiency control of BLDC motor," *IEEE Transactions on Industrial Electronics*, vol. 47, no. 1, pp. 109–114, 2000, doi: 10.1109/41.824132.

[7] R. M. Pindoriya, A. K. Mishra, B. S. Rajpurohit, and R. Kumar, "An analysis of vibration and acoustic noise of BLDC motor drive," in *2018 IEEE Power & Energy Society General Meeting (PESGM)*, Aug. 2018, pp. 1–5, doi: 10.1109/PESGM.2018.8585750.

[8] S. Noguchi and H. Dohmeki, "Improvement of efficiency and vibration noise characteristics depending on excitation waveform of a brushless DC motor," in *2018 IEEE International Magnetics Conference (INTERMAG)*, Apr. 2018, pp. 1–5, doi: 10.1109/INTMAG.2018.8508570.

[9] L. G. Ronauly and S. Riyadi, "A BLDC motor control with variable excitation angle to obtain optimum torque," in *2019 International Conference on Electrical Engineering and Informatics (ICEEI)*, Jul. 2019, pp. 330–335, doi: 10.1109/ICEEI47359.2019.8988897.

[10] J.-H. Yoo and T.-U. Jung, "A study on output torque analysis and high efficiency driving method of BLDC motor," in *2020 IEEE 19th Biennial Conference on Electromagnetic Field Computation (CEFC)*, Nov. 2020, pp. 1–4, doi: 10.1109/CEFC46938.2020.9451336.

[11] S. I. Park, T. S. Kim, S. C. Ahn, and D. S. Hyun, "An improved current control method for torque improvement of high-speed BLDC motor," in *Conference Proceedings - IEEE Applied Power Electronics Conference and Exposition - APEC*, 2003, vol. 1, pp. 294–299, doi: 10.1109/APEC.2003.1179229.

[12] B.-Y. Yang, K.-Y. Hwang, D.-J. Shin, and B.-I. Kwon, "Design of novel magnetic flux barrier for reducing cogging torque in IPM type BLDC motor," *International Journal of Applied Electromagnetics and Mechanics*, vol. 33, no. 1–2, pp. 649–654, Oct. 2010, doi: 10.3233/JAE-2010-1169.

[13] A. Varshney and B. Dwivedi, "Performance analysis of a BLDC drive under varying load," in *2016 IEEE 1st International Conference on Power Electronics, Intelligent Control and Energy Systems (ICPEICES)*, Jul. 2016, pp. 1–4, doi: 10.1109/ICPEICES.2016.7853626.

[14] B. A. kumar, C. Kamal, D. Amudhavalli, and T. Thyagarajan, "Reformed stator design of BLDC motor for cogging torque minimization using finite element analysis," in *2018 4th International Conference on Electrical Energy Systems (ICEES)*, Feb. 2018, pp. 481–484, doi: 10.1109/ICEES.2018.8442389.

[15] J. S. Yoo *et al.*, "Analysis of optimize designing small size BLDC motor considering air gap clearance," in *2018 21st International Conference on Electrical Machines and Systems (ICEMS)*, Oct. 2018, pp. 265–268, doi: 10.23919/ICEMS.2018.8549485.

[16] J.-D. Seo, J.-H. Yoo, and T.-U. Jung, "Design on notch structure of stator tooth to reduce of cogging torque of single-phase BLDC motor," in *2015 18th International Conference on Electrical Machines and Systems (ICEMS)*, Oct. 2015, pp. 1475–1478, doi: 10.1109/ICEMS.2015.7385273.

[17] G. H. Kang, J. Hur, H. G. Sung, and J. P. Hong, "Optimal design of spoke type BLDC motor considering irreversible demagnetization of permanent magnet," in *ICEMS 2003 - Proceedings of the 6th International Conference on Electrical Machines and Systems*, 2003, vol. 1, pp. 234–237.

[18] H.-G. Kim, Jin-Hur, B.-W. Kim, and G.-H. Kang, "Irreversible demagnetization analysis of IPM type BLDC motor considering the circulating current by stator turn fault," in *Digests of the 2010 14th Biennial IEEE Conference on Electromagnetic Field Computation*, May 2010, p. 1, doi: 10.1109/CEFC.2010.5481869.

[19] G.-H. Kang, J. Hur, H. Nam, J.-P. Hong, and G.-T. Kim, "Analysis of irreversible magnet demagnetization in line-start motors based on the finite-element method," *IEEE Transactions on Magnetics*, vol. 39, no. 3, pp. 1488–1491, May 2003, doi: 10.1109/TMAG.2003.810330.

[20] J. Zheng, W. Zhao, C. H. T. Lee, J. Ji, and G. Xu, "Improvement torque performances of interior permanent-magnet machines," *CES Transactions on Electrical Machines and Systems*, vol. 3, no. 1, pp. 12–18, Mar. 2019, doi: 10.30941/CESTEMS.2019.00003.

[21] B.-K Lee, G.-H Kang, J. Hur, and D.-W. You, "Design of spoke type BLDC motors with high power density for traction applications," in *Conference Record of the 2004 IEEE Industry Applications Conference, 2004. 39th IAS Annual Meeting.*, 2004, vol. 2, pp. 1068–1074, doi: 10.1109/IAS.2004.1348545.

[22] Y. Kawase, T. Ota, and H. Fukunaga, "3-D eddy current analysis in permanent magnet of interior permanent magnet motors," *IEEE Transactions on Magnetics*, vol. 36, no. 4, pp. 1863–1866, Jul. 2000, doi: 10.1109/20.877808.

[23] S. Y. Kim, B. T. Kim, J. H. Cho, and J. Lee, "Novel spoke-type BLDC motor design for cost effective and high power density," in *2016 IEEE Transportation Electrification Conference and Expo, Asia-Pacific (ITEC Asia-Pacific)*, Jun. 2016, pp. 90–93, doi: 10.1109/ITEC-AP.2016.7512928.

[24] A. R. Jelani, A. Hitam, J. Jamak, M. Noor, Y. Gono, and O. Ariffin, "antas TM--A tool for the efficient harvesting of oil palm fresh fruit bunches," *Journal of Oil Palm Research*, vol. 20, pp. 548–558, 2016.

[25] M. R. Ahmad, A. R. Jelani, M. Ikmal, and N. Kamarudin, "Oil palm motorised cutter evo2," *MPOB information series*, vol. 2, no. MPOB TT No. 630, pp. 4–7, 2018.

[26] H.-W. Kim, K.-T. Kim, Y.-S. Jo, and J. Hur, "Optimization methods of torque density for developing the neodymium free SPOKE-type BLDC motor," *IEEE Transactions on Magnetics*, vol. 49, no. 5, pp. 2173–2176, May 2013, doi: 10.1109/TMAG.2013.2237890.

[27] R. N. F. Raja Othman *et al.*, "Design of hollow-rotor brushless DC motor," *International Journal of Power Electronics and Drive Systems (IJPEDS)*, vol. 7, no. 2, pp. 387–396, Jun. 2016, doi: 10.11591/ijpeds.v7.i2.pp387-396.

[28] H. K. Kim and J. Hur, "Dynamic Characteristic Analysis of Irreversible Demagnetization in SPM-and IPM-Type BLDC Motors," *IEEE Transactions on Industry Applications*, vol. 53, no. 2, pp. 982–990, 2017, doi: 10.1109/TIA.2016.2619323.

BIOGRAPHIES OF AUTHORS

Muhammad Izanie Kahar received the B. Eng. in Electrical Engineering in 2020 from Universiti Teknikal Malaysia Melaka. Currently, he is pursuing his study in M.Sc. at the same university. His interest of research is analysis in electrical machine. He can be contacted at email: muhammad.izanie@gmail.com.

Raja Nor Firdaus Kashfi Raja Othman received B. Eng., M. Sc. and Ph.D. in Electrical Power Engineering from Universiti Putra Malaysia in 2006, 2009 and 2013, respectively. He is currently associate professor in Department of Electrical Engineering, Faculty of Electrical Technology and Engineering, Universiti Teknikal Malaysia Melaka. His research interest includes applied magnetics, electrical machines, magnetic sensor, and drives. He can be contacted at email: norfirdaus@utem.edu.my.

Aziah Khamis received the B. Eng. degree from Universiti Putra Malaysia in 2006. Then, M. Sc. degree from Newcastle University, U.K. in 2009. Later, Ph.D. degree from Universiti Kebangsaan Malaysia in 2014. She is a senior lecturer at Universiti Teknikal Malaysia Melaka. Her main research interests include intelligent system application of power system study, distributed generation, and microgrid. She can be contacted at email: aziah@utem.edu.my.

Kasrul Abdul Karim received the M.Sc. from University of Bradford and Ph.D. degrees from the University of Nottingham, UK, in 2003 and 2011, respectively. He is currently associate professor at Faculty of Electrical Technology and Engineering, Universiti Teknikal Malaysia Melaka, Durian Tunggal, Malaysia. His research interests include electrical machine design, power electronics, and electric vehicle. He can be contacted at email: kasrul@utem.edu.my.

Fairul Azhar Abdul Shukor received B. Eng in Electrical and Electronic Engineering from Universiti Putra Malaysia in 2002. Then, D. Eng. in Electrical Machine Design from Shinshu University, Nagano, Japan in 2015. He is currently Deputy Dean of Faculty of Electrical Technology and Engineering, Universiti Teknikal Malaysia Melaka. His research interest includes electrical machines, magnetic sensor, machine design, and electric vehicle. He can be contacted at email: fairul.azhar@utem.edu.my.

Ahmad Fuad Ab Ghani received BEng (Hons) degree in Mechanical Engineering from University of Sheffield, United Kingdom in 2004. Further study at University of Manchester, United Kingdom in 2007 obtaining MSc in Maintenance Engineering and Asset Management. Obtained PhD in Mechanical Engineering from Universiti Teknologi Mara (UiTM) in 2019. His research interest is in structural integrity and failure prediction of material using finite element modelling, material characterization and failure study, maintenance engineering and asset management of building, industrial plant, and public facilities. He can be contacted at email: ahmadfuad@utem.edu.my.

Rofizal Mat Rejab graduated in Diploma of Quality Management and having work experiences in machine technology and industry since year of 2000. Currently, he is the managing director of RZtech Resources Sdn. Bhd. which supply and commercialise the technology for oil palm harvesting machinery. He can be contacted at email: rztechresources@gmail.com.